Slow-wave Filters for Millimeter Wave Inter-Satellite Services in Small Satellite Formations

Elígia Simionato, Ana Nora, Marcela Pires, Ivan Aldaya, Ariana L. C. Serrano,
Gustavo P. Rehder and Rafael A. Penchel

***Abstract*— This work focuses on the design of a band-pass filter for the 66 GHz to 71 GHz Inter-Satellite Services band. The design aims to address the need for reliable and efficient inter-satellite communications within small satellite formations, which is considered a promising solution for advancing Beyond-5G communications. The design approach utilizes the slow-wave effect for miniaturization and is compatible with the Metallic-Nanowire-Membrane fabrication platform. A comparison between the slow-wave filter and a traditional microstrip line filter reveals that the slow-wave filter achieves higher selectivity due to the use of higher quality factor slow-wave microstrip lines. Moreover, the slow-wave filter occupies a significantly smaller area, approximately 73% smaller than the traditional approach, demonstrating the advantages of the slow-wave design in terms of miniaturization and improved filter performance.**

***Keywords*— slow-wave, inter-satellite services, millimiter wave, band-pass filters**

I. Introduction

In recent years, there has been a growing pursuit of satellites with increasingly smaller sizes, due to their numerous advantages over traditional larger satellites [1], [2]. Small satellite formations, flying in low-Earth orbits and working as a communication network, represent an attractive solution to support Beyond-5G communications [3]. Furthermore, the seek for small satellites has been driven by the need for cost-effective and agile solutions for various applications such as Earth observation, communication, and scientific research [1]. Small satellite missions have gained significant popularity due to their ability to leverage commercial off-the-shelf technologies, enabling quick and cost-effective mission implementation. These missions offer numerous advantages, including more frequent opportunities for launching, rapid data acquisition, a wide range of mission types, accelerated growth of technical and scientific knowledge, increased participation of small industry, and feasibility for universities. By capitalizing on the benefits of small satellite missions, researchers, scientists, and industry professionals can achieve faster and more readily available access to space, unlocking new possibilities for innovation and exploration [2], [4]–[6].

Elígia Simionato, FESJ/UNESP, São João da Boa Vista - SP, e-mail: e.simionato@unesp.br; Ana Nora, FESJ/UNESP, São João da Boa Vista - SP, e-mail: ana.nora@unesp.br; Marcela Pires, FESJ/UNESP, São João da Boa Vista - SP, e-mail: marcela.p.souza@unesp.br; Ivan Aldaya, FESJ/UNESP, São João da Boa Vista - SP, e-mail: ivan.aldaya@unesp.br. Ariana L. C. Serrano, USP, São Paulo - SP, e-mail: aserrano@usp.br; Gustavo P. Rehder, USP, São Paulo - SP, e-mail: gprehder@usp.br; and Rafael A. Penchel, FESJ/UNESP, São João da Boa Vista - SP, e-mail: rafael.penchel@unesp.br. This work was partially supported by Brazilian agencies São Paulo Research Foundation (FAPESP) under grants #2020/09889-4, #2022/03519-6 and #2022/08613-0; National Council for Scientific and Technological Development (CNPq) under grant #409146/2021-8, and FINEP under grant #0527/18.

One crucial aspect of small satellite systems and formations is the establishment of reliable and efficient inter-satellite communications or Inter-Satellite Services (ISS). As defined by the International Telecommunications Union (ITU), ISS consists of a radiocommunication service that provides links between artificial satellites [7]. ISS are essential for extending networking to space, enabling autonomous data transfer, and functioning as an equivalent to terrestrial Internet, with minimal human intervention. Communication links between satellites provided by ISS facilitate advanced operations such as distributed processing and autonomous applications, eliminating the need for extensive ground-based relay systems and global tracking systems. They also facilitate navigation and formation control through the exchange of attitude and position information, while also ensuring time synchronization between the small satellites [8], [9].

ISS are required to support high-capacity and real-time data transmission, ensuring absolute interoperability among spacecraft within the satellite formation [8]. Meeting these requirements and establishing more efficient interconnections between satellites, as well as preparing for the crescent data volume requirements for known future space science, demands a wider bandwidth [10]. Millimeter wave frequencies, ranging from 30 GHz to 300 GHz, have emerged as a promising solution to address spectrum availability challenges. In fact, one of the bands assigned by ITU to ISS is the 66 GHz to 71 GHz, within the millimeter wave range [11]. This frequency band was identified as highly suitable for ISS due to the atmospheric absorption characteristics, which enable feasible sharing between the ISS and terrestrial services in the 66 GHz to 71 GHz range [11].

However, one of the still ongoing concerns is the potential interference from and to adjacent bands. This interference give systems the potential to significantly impact the performance of ISS or be adversely affected by it [10]. To ensure seamless and interference-free communication between satellites, the integration of filters in satellite systems has become essential. Filters serve as critical components at the RF front-end of satellite transceivers, providing necessary rejection capabilities to protect onboard equipment from unwanted signals and interference sources. Additionally, filters aid in mitigating signal degradation caused by noise, atmospheric interference, and adjacent satellite transmissions [12].

This work presents a design approach for band-pass filters targeting the 66 GHz to 71 GHz ISS band. The proposed design leverages the slow-wave effect to achieve miniaturization of these devices, aligning with the trend towards smaller and more cost-effective satellites. Furthermore, the

design considers compatibility with the Metallic-Nanowire-Membrane (MnM) fabrication platform, which facilitates the implementation of the slow-wave effect.

Section II provides an introduction to the characteristics of the fabrication platform, followed by Section III which explains the principle of the slow-wave effect. The filter design procedure is described in Section IV, and the results of this study are presented and discussed in Section V. Lastly, Section VI concludes this paper.

II. MnM Fabrication Platform

The MnM platform is based on a nanoporous alumina substrate, which offers several advantages. Alumina has excellent insulation properties and exhibits low loss at high frequencies. Moreover, previous studies that utilized MnM technology for millimeter-wave devices demonstrated excellent consistency between measured and simulated results [13]–[16]. The nanoporous alumina is produced by the electrochemical oxidation of aluminum under carefully controlled anodizing voltages. Typically, the nanopores have diameters ranging from 20 nm to 400 nm, with interpore distances varying from a few tenths to a few hundreds of nanometers [13]. In the design of the filters for this work, we used a 50 µm thick alumina membrane, that presents $\epsilon_r = 6.7$ and $\tan\delta = 0.015$.

III. Slow-wave Effect

The slow-wave effect refers to the reduction of the phase velocity of electromagnetic waves propagating in a transmission line. This leads to an artificially produced high dielectric constant, ultimately resulting in compact transmission lines that can be used to design miniaturized versions of RF devices [13]. In this work, we will explore the slow-wave effect specifically in microstrip lines, that can be modeled ideally by a series inductance per unit length L, and a shunt capacitance per unit length C. Thus, their phase velocity can be defined according to (1) [17].

$$v_\phi = \sqrt{\frac{1}{LC}} = \frac{c}{\sqrt{\epsilon_{\text{r,eff}}}} = \frac{\omega d}{\phi} \tag{1}$$

From (1), it is possible to infer that an increase in either L or C will result in an increase of $\epsilon_{\text{r,eff}}$, generating the slow-wave effect. Thus, compared to a traditional microstrip line, a shorter length d is required for the same electrical length ϕ, at a given angular frequency ω [17].

In a slow-wave transmission line, the electric field created between the microstrip and the ground plane is captured by grounded nanowires, which become mostly concentrated in the dielectric (SiO_2) layer, as illustrated in Figure 1. This results in an increase of C. However, the magnetic field can pass through the nanowires with little disturbance due to their small diameter, much smaller than the skin depth at millimeter waves [17]. This means that the value of L in (1) remains almost the same as in a traditional microstrip line. This results in the phase velocity of a slow-wave microstrip being lower than that of a conventional microstrip [17], [18].

This slow-wave effect is simple to acquire with the MnM platform, as the alumina substrate features nanopores that can be filled with copper through an electrodeposition process, forming very thin nanowires [19]. Other technologies, such as printed circuit boards (PCBs), present relatively large vias spaced too far apart that fail to completely confine the electric field in the top dielectric layer, thus reducing the slow-wave effect and increasing propagation loss [18].

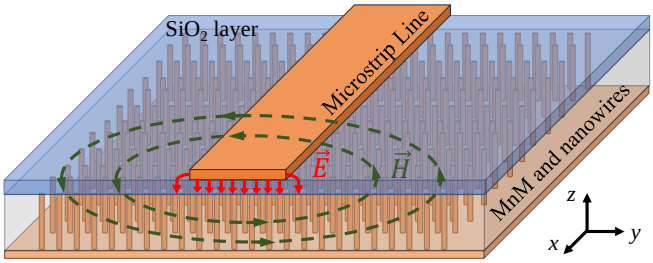

Fig. 1: Illustration of the slow-wave effect on the MnM platform.

For the simulations, it is computationally too costly to include very thin individual nanowires in the geometry. Therefore, we used a block of the same alumina material in the MnM platform ($\epsilon_r = 6.7$ and $\tan\delta = 0.015$) with an anisotropic conductivity condition to mimic the nanowires and capture the electric field, confining it in a thin layer of SiO_2. The anisotropic conductivity considers zero conductivity in the x and y directions (refer to Figure 1), while the z direction has non-zero values, adjusted to accurately model the losses reported by measurements in [18].

IV. Microstrip Band-pass Filter Design Procedure

Multiple implementation techniques for band-pass filters have already been broadly explored in the literature [20], [21]. However, since the aim of this work is to demonstrate the miniaturization capabilities of slow-wave microstrip lines, we decided to use $\lambda_g/2$ open-circuited stubs for implementing the filters, as illustrated in Figure 2. The stubs consist of two sections, each having admittances Y_{ia} and Y_{ib}, and a length of $\lambda_g/4$, denoted as ℓ_{ia} and ℓ_{ib} in Figure 2. The stubs are interconnected by $\lambda_g/4$ sections, indicated as $\ell_{i,i+1} = \lambda_g/4$, with admittances $Y_{i,i+1}$. This technique offers some degree of versatility, while remaining simple to perform.

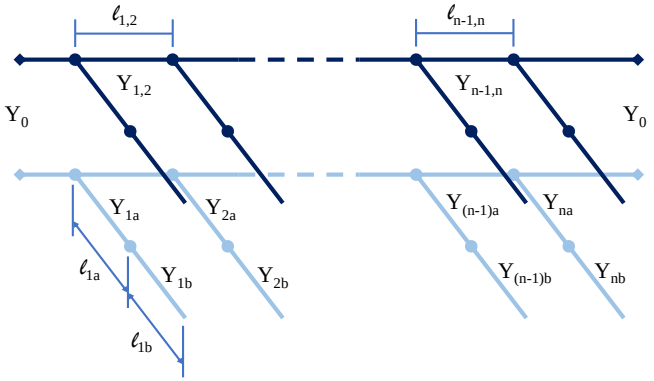

Fig. 2: Band-pass filter with $\lambda_g/2$ open-circuited stubs

The procedure to implement a band-pass filter with $\lambda_g/2$ open-circuited stubs is described in [20] and [21]. For ease of

use, the described technique has been translated into a routine, which is presented as a pseudocode in Algorithm 1.

ALGORITHM 1

Inputs:
Fractional frequency bandwidth (FBW)
Element values (g_i) of the desired filter response
Value of input/output admittance Y_0 in siemens
Design frequency f_0 in hertz
Transmission-zero frequencies f_{zi} in hertz
Filter order n

Calculate:

$$\theta = \frac{\pi}{2}\left(1 - \frac{\text{FBW}}{2}\right)$$

$$J_{1,2} = Y_0 g_0 \sqrt{\frac{2g_1}{g_2}}$$
$$J_{n-1,n} = Y_0 g_0 \sqrt{\frac{2g_1 g_{n+1}}{g_0 g_{n-1}}}$$
$$J_{i,i+1} = \frac{2g_0 g_1}{\sqrt{g_i g_{i+1}}}, \text{ for } i = 2 \text{ to } n-2$$

$$N_{i,i+1} = \left[\left(\frac{J_{i,i+1}}{Y_0}\right)^2 + \left(\frac{2g_0 g_1 \tan\theta}{2}\right)^2\right]^{1/2}, \text{ for } i = 1 \text{ to } n-1$$

$$Y_1 = Y_0\left(N_{1,2} - \frac{J_{1,2}}{Y_0}\right)$$
$$Y_n = Y_0(g_n g_{n+1} - g_0 g_1)\tan\theta + Y_0\left(N_{n-1,n} - \frac{J_{n-1,n}}{Y_0}\right)$$
$$Y_i = Y_0\left(N_{i-1,i} + N_{i,i+1} + \frac{J_{i-1,i}}{Y_0} + \frac{J_{i,i+1}}{Y_0}\right), \text{ for } i = 2 \text{ to } n-1$$
$$Y_{i,i+1} = J_{i,i+1}, \text{ for } i = 1 \text{ to } n-1$$

$$\alpha_i = \cot^2\left(\frac{\pi f_{zi}}{2f_0}\right), \text{ for } f_{zi} < \text{low band-edge frequency}$$
$$Y_{ia} = Y_i\frac{(\alpha_i \tan^2\theta - 1)}{(\alpha_i + 1)\tan^2\theta}$$
$$Y_{ib} = \alpha_i Y_{ia}$$

$$Z_{i,i+1} = 1/Y_{i,i+1}\ [\Omega]$$
$$Z_{ia} = 1/Y_{ia}\ [\Omega]$$
$$Z_{ib} = 1/Y_{ib}\ [\Omega]$$

Outputs:
Connecting lines impedances $Z_{i,i+1}$
Stubs impedances Z_{ia} and Z_{ib}

The versatility of this technique relies on the choosing of the transmission-zero or attenuation-pole frequencies f_{zi}. It is permissible to adjust f_{zi} for each stub, resulting in broader regions of high rejection, although maintaining the same f_{zi} for all stubs would give the best passband response [20]. In this work, we used f_{zi} to adjust the required stub impedances to be at a viable range for microstrip implementation.

We opted to implement a fifth-order filter with a Butterworth (maximally flat) response. Although this filter type does not offer high frequency selectivity, it ensures a flat transmission to avoid introducing signal distortions [22]. For operation within the 66 GHz to 71 GHz band, we have FBW = 0.072. The element values for the selected filter and the resulting impedances are presented in Table I. The input and output ports, corresponding to a 50 Ω impedance, are denoted as $i = 0$ and $i = 6$, respectively.

Based on the impedance values provided in Table I, we determined the dimensions of the traditional microstrip lines using standard formulations [22]. The dimensions of the slow-wave microstrip lines were determined through simulation. To achieve the desired impedances, a parametric analysis of the slow-wave microstrip width was conducted, considering a 2 µm thick SiO_2 layer, which provided a suitable range of impedance values. The $\lambda_g/4$ lengths were determined by considering the effective dielectric constant $\epsilon_{\text{r,eff}} \equiv [c\beta/(2\pi f)]^2$, which was obtained by calculating the propagation constant γ using the transmission matrix elements, as described in [23]. The geometries of the resulting filters are shown in Figure 3.

TABLE I: Element values and impedances for a fifth-order Butterworth filter

i	0	1	2	3	4	5	6
g	1	1.1468	1.3712	1.975	1.3712	1.1468	1
$Z_{i,i+1}$ [Ω]	50	57.21	72.77	72.77	57.21	50	–
Z_{ia} [Ω]	–	18.54	14.21	14.16	14.21	18.54	–
Z_{ib} [Ω]	–	50.13	66.67	66.84	66.67	50.13	–

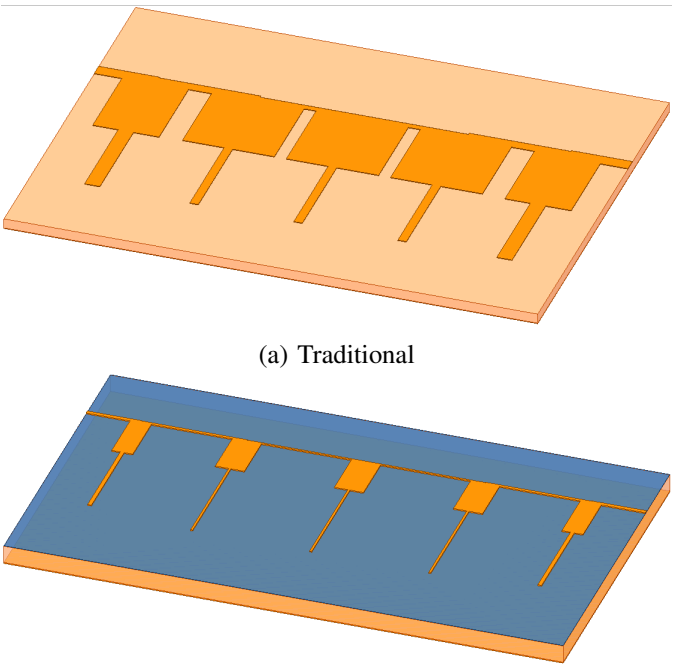

(a) Traditional

(b) Slow-wave

Fig. 3: Designed filters' geometry.

The traditional filter occupies an area of 2.62 mm^2, whereas the slow-wave filter occupies a significantly smaller area of only 0.714 mm^2, which is 73% smaller. This highlights the significant reduction in size achieved by the slow-wave filter design compared to the traditional approach.

V. Numerical Analysis and Results

The performance evaluation of the designed filters was conducted using Ansys High Frequency Structure Simulator (HFSS). The results, illustrated in Figures 4 and 5, show the performance of both the slow-wave filter and the filter using traditional microstrip lines. The dashed lines in Figure 4

represent the desired bandwidth limits, and it can be observed that the slow-wave filter demonstrates higher selectivity in comparison to the traditional microstrip filter. Figure 5, which shows the filters' response in a wider bandwidth, reveals that both filters have a wide stop band, but the slow-wave filter achieves higher stop band attenuation. However, the slow-wave filter also exhibits 2 dB higher attenuation in the pass band. The high and low cutoff frequencies ($f_{3\text{dB,H}}$ and $f_{3\text{dB,L}}$, respectively), as well as the slope and pass band attenuation values for each filter, are presented in Table II.

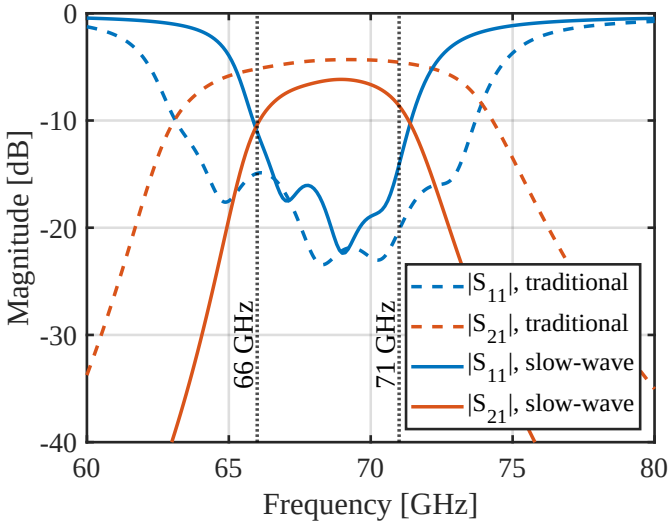

Fig. 4: Filters' response at the desired frequency band.

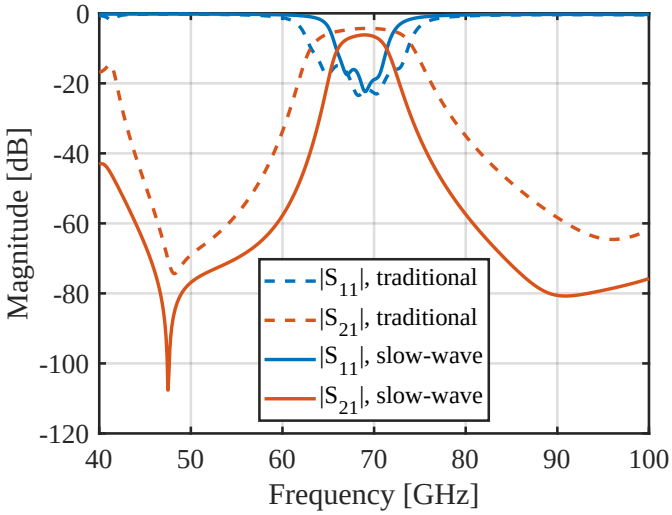

Fig. 5: Filters' response analyzed in a wider frequency range.

TABLE II: Designed filters' characteristics

	Slow-wave	**Traditional**
$f_{3\text{dB,L}}$	66.29 GHz	63.96 GHz
$f_{3\text{dB,H}}$	71.14 GHz	73.57 GHz
Slope	-40dB/decade	-20dB/decade
Pass band attenuation	6.2 dB	4.3 dB

From Table II, it is evident that the cutoff frequencies of the slow-wave filter closely align with the desired bandwidth limits. In contrast, the filter employing a traditional microstrip line exhibits a bandwidth that is approximately 4 GHz broader than the intended range.

The increased frequency selectivity achieved by the slow-wave filter is due to the increased capacitive effect in the microstrip lines, discussed in Section III. This can also be understood in terms of the quality factor. In filters, the quality factor is determined by the center frequency f_C and the 3 dB bandwidth, as described by (2). In microstrip lines, the quality factor establishes a relationship between the phase constant β and the attenuation constant α, and can also be expressed in terms of the phase velocity v_ϕ, as demonstrated by (3).

$$Q_{\text{filter}} = \frac{f_C}{f_{3\text{dB,H}} - f_{3\text{dB,L}}} = \frac{f_C}{\text{BW}_{3\text{dB}}} \tag{2}$$

$$Q_{\text{lines}} = \frac{\beta}{2\alpha} = \frac{\omega}{2\alpha v_\phi} \tag{3}$$

According to the principle of the slow-wave effect (see Section III), the phase velocity v_ϕ decreases, leading to an increase in the phase constant β and subsequently the quality factor. However, it was observed that the slow-wave line exhibits higher losses, as indicated in Table II, which is a result of a higher attenuation constant α compared to the traditional microstrip line. Nevertheless, the slower phase velocity and the corresponding higher phase constant β have a more significant impact than the increase in α when compared to the traditional microstrip line, as shown in Figure 6. This ultimately leads to the aforementioned higher quality factor, as demonstrated in Figure 7.

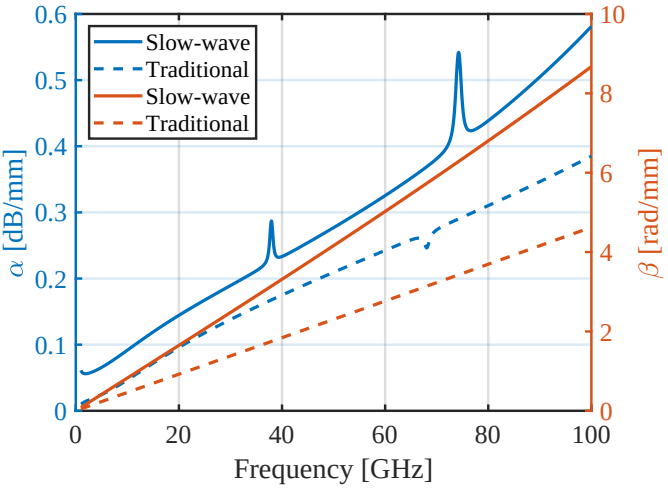

Fig. 6: 50 Ω microstrips α and β.

The implementation of microstrip lines with a higher quality factor results in a filter with an increased quality factor as well. As stated in (2), this results in a narrower 3 dB bandwidth, which corresponds to higher selectivity, as demonstrated by Figure 4.

VI. Conclusions

This work presented two designs for a band-pass filter targeting the 66 GHz to 71 GHz Inter-Satellite Services band.

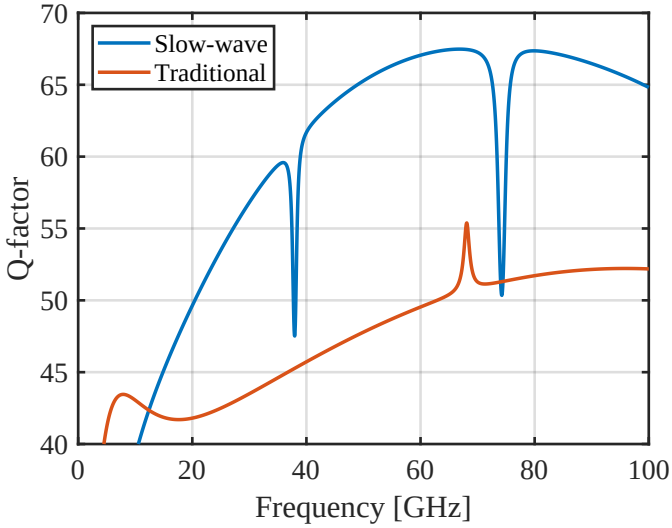

Fig. 7: 50 Ω microstrips quality factor.

One design implemented traditional microstrip lines, while the other design employed the slow-wave effect as a miniaturization technique, aligning with the trend towards smaller and more cost-effective satellites. A comparative analysis between the slow-wave filter and a traditional microstrip line filter has revealed that the slow-wave filter achieves the desired bandwidth as a result of its higher selectivity, attributed to the utilization of slow-wave microstrip lines with higher quality factor. Additionally, the slow-wave filter offers a substantial reduction in size, occupying an area approximately 73% smaller than the traditional approach.

REFERENCES

[1] S. A. Catapult, "Small Satellite Report Q4 2021." https://sa.catapult.org.uk/wp-content/uploads/2022/05/22021615-Small-Sat-Report-Q4-2021_fin.pdf, 2022. [Online].

[2] R. Sandau, K. Brieß, and M. D'Errico, "Small satellites for global coverage: Potential and limits," *ISPRS Journal of Photogrammetry and Remote Sensing*, vol. 65, pp. 492–504, Nov. 2010.

[3] I. Leyva-Mayorga, B. Soret, M. Röper, D. Wübben, B. Matthiesen, A. Dekorsy, and P. Popovski, "Leo small-satellite constellations for 5g and beyond-5g communications," *IEEE Access*, vol. 8, pp. 184955–184964, 2020.

[4] M. I. Rashed and H. Bang, "A Study of Autonomous Small Satellite Constellations for Disaster Management and Deep Space Strategy," *Remote Sensing*, vol. 14, Jan. 2022. Number: 23 Publisher: Multidisciplinary Digital Publishing Institute.

[5] N. H. Crisp, K. L. Smith, and P. M. Hollingsworth, "An integrated design methodology for the deployment of constellations of small satellites," *The Aeronautical Journal*, vol. 123, pp. 1193–1215, Aug. 2019. Publisher: Cambridge University Press.

[6] D. J. Barnhart, T. Vladimirova, A. M. Baker, and M. N. Sweeting, "A low-cost femtosatellite to enable distributed space missions," *Acta Astronautica*, vol. 64, pp. 1123–1143, June 2009.

[7] International Telecommunication Union (ITU), "ITU-R Radio Regulations." https://www.itu.int/en/publications/ITU-R/pages/publications.aspx?media=electronic&parent=R-REG-RR-2020, 2020. [Online].

[8] R. Radhakrishnan, W. W. Edmonson, F. Afghah, R. M. Rodriguez-Osorio, F. Pinto, and S. C. Burleigh, "Survey of Inter-Satellite Communication for Small Satellite Systems: Physical Layer to Network Layer View," *IEEE Communications Surveys & Tutorials*, vol. 18, no. 4, pp. 2442–2473, 2016. Conference Name: IEEE Communications Surveys & Tutorials.

[9] N. Herscovici, C. Christodoulou, V. Lappas, G. Prassinos, A. Baker, and R. Magnuss, "Wireless Sensor Motes for Small Satellite Applications," *IEEE Antennas and Propagation Magazine*, vol. 48, pp. 175–179, Oct. 2006. Conference Name: IEEE Antennas and Propagation Magazine.

[10] I. T. U. (ITU), "ITU-R CPM Report 2023." https://www.itu.int/dms_pub/itu-r/opb/act/R-ACT-CPM-2023-PDF-E.pdf, 2023. [Online].

[11] International Telecommunication Union (ITU), "Recommendation ITU-R S.1327 Requirements and Suitable Bands for Operation of the Inter-Satellite Service Within the Range 50.2-71 GHz." https://www.itu.int/rec/R-REC-S.1327-0-199709-I/en, 1997. [Online].

[12] F. De Paolis, "Satellite filters for 5g/6g and beyond," in *2021 IEEE MTT-S International Microwave Filter Workshop (IMFW)*, pp. 148–150, 2021.

[13] M. V. Pelegrini, J. M. Pinheiro, L. G. Gomes, G. P. Rehder, A. L. C. Serrano, F. Podevin, and P. Ferrari, "Interposer based on metallic-nanowire-membrane (MnM) for mm-wave applications," in *2016 11th European Microwave Integrated Circuits Conference (EuMIC)*, pp. 532–535, Oct. 2016.

[14] J. E. G. Lé, M. Ouvrier-Buffet, L. G. Gomes, R. A. Penchel, A. L. C. Serrano, and K. G. P. Rehder, "Integrated Antennas on MnM Interposer for the 60 GHz Band," *Journal of Microwaves, Optoelectronics and Electromagnetic Applications*, vol. 21, pp. 184–193, Mar. 2022.

[15] L. A. G. Gomes, *Projeto de antenas e caracterização do substrato de nanofios (MnM) para aplicações em ondas milimétricas.* text, Universidade de São Paulo, Dec. 2017.

[16] E. Simionato, B. M. Verona, M. Pires de Souza, I. Aldaya, J. de Oliveira, A. Serrano, G. P. Rehder, and R. A. Penchel, "Design and analysis of a butler matrix at 60 GHz compatible with Metallic-Nanowire-Filled membrane fabrication platform," in *XL Simpósio Brasileiro de Telecomunicações e Processamento de Sinais (SBrT 2022)*, (Santa Rita do Sapucaí, Brazil), Sept. 2022.

[17] A. L. C. Serrano, A.-L. Franc, D. P. Assis, F. Podevin, G. P. Rehder, N. Corrao, and P. Ferrari, "Slow-wave microstrip line on nanowire-based alumina membrane," in *2014 IEEE MTT-S International Microwave Symposium (IMS2014)*, pp. 1–4, June 2014. ISSN: 0149-645X.

[18] A. L. C. Serrano, A.-L. Franc, D. P. Assis, F. Podevin, G. P. Rehder, N. Corrao, and P. Ferrari, "Modeling and Characterization of Slow-Wave Microstrip Lines on Metallic-Nanowire- Filled-Membrane Substrate," *IEEE Transactions on Microwave Theory and Techniques*, vol. 62, pp. 3249–3254, Dec. 2014.

[19] G. Acri, *Sensitivity to technology and adjustability of substrate integrated waveguides Butler matrices, in PCB substrates at 28 GHz and in benzocyclobutene above-IC interposers at millimetre waves*. PhD thesis, July 2020.

[20] Jia-Sheng Hong and M. J. Lancaster, *Lowpass and Bandpass Filters*, ch. 5, pp. 109–159. John Wiley & Sons, 2001.

[21] G. Mattaei, L. Young, and E. M. T. Jones, *Microwave Filters, Impedance-Matching Networks, and Coupling Structure*. Artech House, Norwood, 1980.

[22] D. M. Pozar, *Microwave Engineering*. John Wiley & Sons, 2011.

[23] A. Mangan, S. Voinigescu, M.-T. Yang, and M. Tazlauanu, "De-embedding transmission line measurements for accurate modeling of IC designs," *IEEE Transactions on Electron Devices*, vol. 53, pp. 235–241, Feb. 2006. Conference Name: IEEE Transactions on Electron Devices.